LOW-SPEED AIRFOIL SECTION RESEARCH
AT DELFT UNIVERSITY OF TECHNOLOGY

J.L. van Ingen, L.M.M. Boermans and J.J.H. Blom
Department of Aerospace Eng., Delft University of Technology
Kluyverweg 1, 2629 HS Delft, the Netherlands

Summary

A review is given of some theoretical and experimental research on the aerodynamic characteristics of airfoil sections for low speed flows.
Computer programs have been developed which combine potential flow calculations with other computational methods to predict the development of the laminar boundary layer, the occurrence and possibly bursting of laminar separation bubbles, the position of transition and the development of the turbulent boundary layer.
Special attention has been given to theoretical and experimental research on the subjects of laminar separation bubbles and transition. The paper will review the main results of this research.
Capabilities of the resulting computer programs will be illustrated through comparison with experimental results for some airfoils.

1. Introduction

The choice of airfoils for specific applications has long been determined by experimental investigations. The designer has been extensively supported by such reference works as the NACA airfoil catalogues containing a wealth of experimental results.
With the advent of modern computational tools it has become possible to design a special airfoil for each specific application. For low speed flows the pioneering work of R. Eppler and F.X. Wortmann should be mentioned.
The work at the Delft University of Technology Low Speed Laboratory (LSL) on airfoil analysis and design was started by the first author during a sabbatical leave, spent at the Lockheed Georgia Company in 1966-1967. A prototype computerprogram was put together, based on the then available computational methods for viscous flows and the conformal transformation method due to Timman[1].
A description of this program may be found in [2,3]. A special feature of this program was the so-called e^9 transition prediction method, based on linear stability theory, which was developed independently by Smith and Gamberoni[4] and Van Ingen[5,6].
Later it became clear that for low speed flows the formation and bursting of laminar separation bubbles needed further detailed experimental investigations.

Over the years a number of computational tools for low speed airfoil analysis and design has been developed at LSL; in addition experimental research on related topics has been performed. The present paper gives an overview of this work.

2. Computational tools for two-dimensional potential flows

2.1. Direct and inverse methods based on conformal transformation of the flow around a circle into the flow around a single-element airfoil

It is easy to transform the potential flow around

a circle in the ζ-plane into the flow around a single-element airfoil in the z-plane if a transformation function is specified. The well-known Joukowsky transformation is given by equation (1) through (3) in table 1, where b is a real positive constant. In the points $\zeta = +b$ the derivative $\frac{dz}{d\zeta}$ is equal to zero which means that the transformation is not conformal there. Choosing a circle passing through the point $\zeta = +b$ which encloses the point $\zeta = -b$ (fig. 1) produces an airfoil with a cusped trailing edge at the point $z = +2b$. By varying the position of the center of the circle in the ζ-plane a two-parameter family of airfoils is obtained with variable thickness and camber and cusped trailing-edges.
A three-parameter family of airfoils with an arbitrary non-zero trailing-edge angle δ may be obtained from the von Kármán-Trefftz transformation (equations 4 through 6 in table 1).
In equations (1) through (6) b and k are real positive constants; k is slightly less than 2 and is related to the trailing-edge angle δ by

$$k = 2 - \frac{\delta}{\pi} \tag{10}$$

A not so well-known transformation function – which however is very handy in applications – is due to Müller[7] (equations 7 through 9 in table 1). Here b and k have the same meaning as for the von Kármán-Trefftz transformation. The resulting airfoils are very similar; the algebra however is somewhat simpler for the Müller airfoils (for an example see fig. 2). By increasing the number of parameters, or by applying a series of successive transformations, a great variety of airfoils may be obtained. A review of these transformations has been given by Blom[8]. It is however not possible to obtain an arbitrarily specified airfoil in this way.
Numerical methods which transform a circle into an arbitrarily specified airfoil have been developed by Theodorsen[9], Goldstein[10], Lighthill[11], Timman[1] and others.
We will discuss here in some detail Timman's method because this has become one of the computational tools at LSL.

In what follows we will take a circle (radius R) in the ζ-plane with its center in the origin in a uniform flow with velocity U_∞ under an angle of attack α with respect to the horizontal axis (fig. 3). Choosing the circulation Γ such that the rear stagnation point is found at $\theta = \theta_{st}$, we find

$$\Gamma = 4\pi R U_\infty \sin(\alpha - \theta_{st}) \tag{11}$$

The velocity on the contour of the circle is given by

$$U_c = 2U_\infty[\sin(\theta - \alpha) + \sin(\alpha - \theta_{st})] \tag{12}$$

Joukowsky	$z = \zeta + \dfrac{b^2}{\zeta}$	(1)
	$\dfrac{z - 2b}{z + 2b} = \left(\dfrac{\zeta - b}{\zeta + b}\right)^2$	(2)
	$\dfrac{dz}{d\zeta} = 1 - \dfrac{b^2}{\zeta^2} = \left(1 - \dfrac{b}{\zeta}\right)\left(1 + \dfrac{b}{\zeta}\right)$	(3)
von Kármán-Trefftz	$\dfrac{z - kb}{z + kb} = \dfrac{(\zeta - b)^k}{(\zeta + b)^k}$	(4)
	$z = \zeta + \dfrac{k^2 - 1}{3}\dfrac{b^2}{\zeta} - \dfrac{(k^2 - 1)(k^2 - 4)}{45}\dfrac{b^4}{\zeta^3} + \dfrac{(k^2 - 1)(k^2 - 4)(2k^2 - 11)}{945}\dfrac{b^6}{\zeta^5} + \ldots$	(5)
	$\dfrac{dz}{d\zeta} = 1 - \dfrac{k^2 - 1}{3}\left(\dfrac{b}{\zeta}\right)^2 + \dfrac{(k^2 - 1)(k^2 - 4)}{15}\left(\dfrac{b}{\zeta}\right)^4 - \dfrac{(k^2 - 1)(k^2 - 4)(2k^2 - 11)}{189}\left(\dfrac{b}{\zeta}\right)^6 + \ldots$	(6)
Müller	$z = \zeta\left(1 - \dfrac{b}{\zeta}\right)^k + kb$	(7)
	$z = \zeta + \dfrac{k(k - 1)}{2!}\dfrac{b^2}{\zeta} - \dfrac{k(k - 1)(k - 2)}{3!}\dfrac{b^3}{\zeta^2} + \dfrac{k(k - 1)(k - 2)(k - 3)}{4!}\dfrac{b^4}{\zeta^3} + \ldots$	(8)
	$\dfrac{dz}{d\zeta} = \left(1 - \dfrac{b}{\zeta}\right)^{k-1}\left[1 + (k - 1)\dfrac{b}{\zeta}\right]$	(9)

Table 1: Some classical conformal transformations.

We will choose the conformal transformation such that the point $\theta = 0$ on the circle is mapped into the sharp trailing-edge of the airfoil.
The well-known Kutta condition then requires that $\theta_{st} = 0$ for potential flow leading to

$$\Gamma_{pot\ flow} = 4\pi R U_\infty \sin \alpha \qquad (13)$$

and

$$Uc_{pot\ flow} = 2U_\infty[\sin(\theta - \alpha) + \sin \alpha] \qquad (14)$$

The lift in potential flow will then be zero for $\alpha = 0$. Later on we will apply a correction to the lift for viscous effects which will be effected by allowing the stagnation point to move away from $\theta = 0$ to a small value $\theta_{st} \neq 0$ (see section 3.5.). In that case equations (11) and (12) will be used.

The transformation function

$$z = f(\zeta) \qquad (15)$$

will be chosen such that the flow fields at infinity are the same in both planes. This means that also the lift on the airfoil will be zero for $\alpha = 0$. In other words the airfoil will appear in the z-plane in such an attitude that the free-stream direction for zero lift is horizontal.
In what follows two real functions σ and τ will be used, they are defined by

$$\frac{dz}{d\zeta} = e^{\sigma + i\tau} \qquad (16)$$

Since σ and τ are the real- and imaginary parts of an analytic function they are related to each other; on the circle the relation is given by the well known Poisson integral. Taking the absolute value of (16) it follows that the ratio of the length of a line-element $|dz|$ in the z-plane to the length of the corresponding element $|d\zeta|$ in the ζ-plane follows from

$$|dz| = e^\sigma |d\zeta| \qquad (17)$$

Taking the argument of (16) it follows that $d\zeta$ has to be turned over an angle τ to obtain the direction of dz. We will take the complex potential equal in corresponding points of both planes. Hence the ratio of the magnitudes of the velocity in both planes is inversely proportional to the ratio of the lengths of the line-elements. Hence

$$|U_a| = e^{-\sigma} |U_c| \qquad (18)$$

The most general form of the transformation leaving the flow field at infinity unchanged is given by

$$z = \zeta + C_0 + \frac{C_1}{\zeta} + \frac{C_2}{\zeta^2} + \frac{C_3}{\zeta^3} + \ldots + \frac{C_n}{\zeta^n} + \ldots \qquad (19)$$

or

$$\frac{dz}{d\zeta} = 1 - \frac{C_1}{\zeta^2} - \frac{2C_2}{\zeta^3} - \frac{3C_3}{\zeta^4} \ldots - \frac{nC_n}{\zeta^{n+1}} + \ldots \qquad (20)$$

402

The coefficients C_n in (19) and (20) are in general complex. The fact that in (20) no term with ζ^{-1} occurs, ensures that a closed airfoil is obtained in the z-plane. It can be shown that this also means that σ and τ on the circle have to satisfy the following set of "closing conditions" (see e.g. (2).

$$\left.\begin{array}{l} \displaystyle\int_0^{2\pi} \sigma(\theta)\, d\theta = 0 \\[2mm] \displaystyle\int_0^{2\pi} \sigma(\theta)\cos\theta\, d\theta = 0 \\[2mm] \displaystyle\int_0^{2\pi} \sigma(\theta)\sin\theta\, d\theta = 0 \end{array}\right\} \qquad (21a)$$

$$\left.\begin{array}{l} \displaystyle\int_0^{2\pi} \tau(\theta)\, d\theta = 0 \\[2mm] \displaystyle\int_0^{2\pi} \tau(\theta)\cos\theta\, d\theta = 0 \\[2mm] \displaystyle\int_0^{2\pi} \tau(\theta)\sin\theta\, d\theta = 0 \end{array}\right\} \qquad (21b)$$

Later on these relations will become important when we try to calculate σ and τ for a given airfoil or when we want to modify a given airfoil to obtain an improved pressure distribution.

When σ is known on the contour of the circle the velocity on the airfoil contour follows from (12) and (18):

$$U_a = 2e^{-\sigma}\, U_\infty [\sin(\theta - \alpha) + \sin(\alpha - \theta_{st})] \qquad (22)$$

The circulation around the airfoil is the same as that around the circle given by (11). When the airfoil chord is denoted by c, the airfoil lift coefficient follows from

$$c_\ell = 8\pi\,\frac{R}{c}\,\sin(\alpha - \theta_{st}) \qquad (23)$$

and the lift curve slope $\dfrac{\partial c_\ell}{\partial \alpha}$ from

$$\frac{\partial c_\ell}{\partial \alpha} = 8\pi\,\frac{R}{c}\,\cos(\alpha - \theta_{st})\left(1 - \frac{\partial\theta_{st}}{\partial\alpha}\right) \qquad (24)$$

For thin airfoils we should obtain 2π for $\dfrac{\partial c_\ell}{\partial\alpha}$ so that we can expect

$$c \approx 4R \qquad (25)$$

Denoting $\dfrac{\partial\theta_{st}}{\partial\alpha}$ by ε we have

$$\frac{\partial c_\ell}{\partial\alpha} = 8\pi\,\frac{R}{c}\,\cos(\alpha - \theta_{st})\,(1 - \varepsilon) \qquad (26)$$

and for small $(\alpha - \theta_{st})$

$$\frac{\partial c_\ell}{\partial\alpha} = 8\pi\,\frac{R}{c}\,(1 - \varepsilon) \qquad (27)$$

In potential flow we have $\theta_{st} = 0$ and hence $\varepsilon = 0$; the ratio of the lift curve slope in viscous flow ($\varepsilon \neq 0$) to that in potential flow ($\varepsilon = 0$) then is $(1 - \varepsilon)$.

Once σ and τ are known as functions of θ on the circle the geometry of the airfoil is easily recovered from an integration of (16). On the other hand the pressure distribution follows from (22). This strongly recommends to use σ and τ as primary functions describing the airfoil rather than using the coordinates. It should be observed that σ and τ on the circle are related by Poisson's integral so that one function determines the other. In the numerical applications of the method we always use a discretization in which e^σ and τ are determined in 100 points equally spaced around the circle. The Poisson integrals are then replaced by finite sums over these 100 function values; the coefficients in the sums only depending on the number of points being used. Since $\frac{dz}{d\zeta}$ is zero at the sharp trailing-edge $e^\sigma \to 0$ and hence $\sigma \to -\infty$ there. Moreover τ has a discontinuity equal to $2\pi - \delta$ at the trailing-edge. In numerical applications the singularity at the trailing-edge is avoided by performing the numerical computations only on the differences between σ (and τ) for the given airfoil and a von Kármán-Trefftz or Müller airfoil having the same trailing-edge angle. The singular behaviour near the trailing edge can then be handled analytically using (4) through (10).

To find the characteristic functions σ and τ for a given airfoil we start with an approximative von Kármán-Trefftz or Müller airfoil having the same trailing-edge angle. Then corrections $\Delta\sigma$ and $\Delta\tau$ are obtained in an iterative way until the approximative airfoil is deformed into the given airfoil. To ensure a closed airfoil the closing conditions (21a) and (21b) are enforced at each step in the iteration. The whole proces converges very fast in general. Typical CPU times on an IBM 370-158 are 2.5 seconds for a symmetrical airfoil and 4.0 seconds for a cambered airfoil. An example is given in fig. 4 where the NACA 0012 airfoil is obtained in a few steps. To show the rapid convergence a very thick initial von Kármán-Trefftz airfoil has been chosen. Once the final values for e^σ and τ in 100 points around the circle have been obtained they are stored in a computer library for future use.

Often the designer will not be satisfied with the characteristics of a given airfoil and he may want to change the functions σ and τ (and hence the airfoil geometry) such that an improved pressure distribution is obtained. This can be done as follows. Let the pressure distribution for the existing airfoil be known at a certain value of the angle of attack and let it be plotted in the form of

$$\bar{U} = \frac{|U_a|}{U_\infty} \qquad (28)$$

versus θ. The designer now may want to change this curve in a certain interval to the curve ----------- indicated in fig. 5. Then the existing and proposed values of $\bar{U}$ define a correction $\Delta\sigma(\theta)$ to $\sigma(\theta)$ by the following equation, derived from (18),

$$\Delta\sigma(\theta) = -\ln \left| \bar{u}_{proposed}/\bar{u}_{existing} \right| \qquad (29)$$

It should be remembered that arbitrary modifications to σ are not allowed because these might violate the closing conditions (21a). Therefore the computer program applies a filtering proces to the proposed function $\Delta\sigma(\theta)$ to remove the unacceptable lower harmonics.
The result is a permissible function $\Delta\sigma$ and hence also a permissible new pressure distribution (— — — in fig. 5). Once the correction $\Delta\sigma$ is known the corresponding correction $\Delta\tau$ follows from the numerical approximation to the Poisson integral, the corrected functions σ and τ define the new airfoil. For a detailed description of this procedure the reader is referred to (2). An example is given in fig. 6 where the pressure distribution for NACA 0012 at α = 0 is modified into one of the laminar flow type.

2.2. Singularity distributions on single- or multi-element airfoils and windtunnel walls

In many applications today methods are employed which are based on the idea of putting singularities such as sources/sinks, vortices and/or dipoles inside or on the airfoil contour. The strength of the singularities is chosen in such a way that the contour becomes a streamline. Numerically these methods reduce the problem to the solution of a set of linear algebraic equations. They have the advantage over conformal transformation methods of being readily extendable to multi-element airfoils and three dimensional wings. Sometimes numerical problems arise for very thin airfoils or near thin trailing edges.
At LSL we use a method programmed by Gooden[12] in which contours are replaced by a polygon; each element is provided with a linearly varying vorticity distribution.
Using such a method it is easy to determine the effect of windtunnel walls on the pressure distribution around an airfoil by also covering the walls with vortex panels.

2.3. Combination of the methods of conformal transformation and singularity distributions

The numerical problems, which may arise in the method of singularity distributions for thin airfoils and/or thin trailing-edges can be removed by opening up the sharp trailing-edge to an angle of 180 degrees by means of a conformal transformation. At LSL we use an inverse von Kármán-Trefftz or a Müller transformation for this purpose; the airfoil is then transformed into a nearly circular contour. The numerical treatment is now easier than for the airfoil contour for two reasons. In the first place the singular behaviour near the trailing-edge is described by the transformation which can be handled analytically. Secondly the singularity distribution on the nearly circular contour behaves much smoother than on the airfoil contour. Therefore the number of vortex panels – and hence the number of linear algebraic equations to solve – can be greatly reduced.
Figs. 7 through 9 give some examples of application of this procedure. Fig. 7 gives the transformation of the Wortmann FX66-S-196V1 airfoil into a near circle; fig. 8 shows the same procedure applied to the very thin Eppler 377 airfoil. The pressure distributions calculated in this way and by Timman's

method are so nearly the same that differences cannot be shown on a graph of reasonable size. The same transformation can be applied to multi-element airfoils. Fig. 9 shows two successive transformations which transform a wing and leading-edge slat combination into two nearly circular contours.

2.4. A linearized method for flows around nearly circular contours obtained by conformal transformation from an airfoil

It was mentioned already in section 2.3. that the application of a suitably chosen inverse von Kármán-Trefftz or Müller transformation to an airfoil results in a nearly circular shape. When the distance ε between this contour (C_1 in fig. 10) and a nearby exact circle (C_2 in fig. 10) is small, the singularity distribution may be put on the circle to generate the flow around the near circle. This has the advantage that the distributions may be described by Fourier series which can be handled very easily by Fast Fourier Transform routines. Assuming small deviations ε between the near circle and the exact circle a linearized method has been developed at LSL. This method has the advantage over the usual linearized airfoil theories that it is also accurate near leading- and trailing-edges. In this method we use a vorticity distribution on the exact circle C_2 to make this circle a streamline in a given onset flowfield w. Then a source distribution on C_2 is added to make the nearly circular contour C_1 a streamline instead of C_2.
The accuracy of this linearized method follows from table 2 where some results are shown for an elliptical contour with semi axes a and b (fig. 11) where the vortex and source distributions have been put on a circle with radius R = 1.

θ degrees	$\dfrac{v - v_{exact}}{v_{exact}}$ in percent				
	a = 1 b = .9	a = 1.1 b = 1.0	a = 1.05 b = 0.95	a = 1.1 b = 0.9	a = 1.2 b = 0.8
18	−.54	−1.24	−0.64	+1.98	−4.76
36	−.11	−0.37	+0.01	0.39	−2.89
54	−.21	+0.12	+0.21	0.74	+1.94
72	−.65	+0.15	+0.00	−0.16	−1.42
90	−.88	+0.09	−0.15	−0.68	−2.91

Table 2: Results of linearized method for elliptical airfoils.

It follows from table 2 that even for rather large deviations from a circle the resulting error is only a few percent. The best results can be expected when ε is partly > 0 and partly < 0, see for instance the case a = 1.05 and b = 0.95 in table 2. In practice we use an approximating circle C_2 with an area equal to the area within the nearly circular contour C_1 with the center of the circle in the centroid of the area enclosed by C_1. It should be noted that in this way the singularities on C_2 sometimes stick out into the flow field outside C_1. This is permissible since the equations used have been derived for the flow outside C_2. Extending its use inside C_2 without taking into account the jumps in normal and tangential velocity which should occur on C_2, just provides us with the proper flowfield outside C_1.

3. Computational methods and experimental research for viscous flows

3.1. The laminar boundary layer

A well known engineering method for the calculation of the laminar boundary layer is that due to Thwaites[13]. The accuracy of the method is quite good for the prediction of the momentum loss thickness θ; it is less accurate for the prediction of the separation position. The idea behind this method is to use the von Kármán momentum integral relation

$$\frac{d}{dx}\left(\frac{\theta^2}{\nu}\right) = \frac{2\ell + 2m(2+H)}{U} = \frac{L}{U} \tag{30}$$

and the first compatibility condition of the boundary layer

$$m = -\frac{\theta^2}{\nu}\frac{dU}{dx} \tag{31}$$

Thwaites assumed that ℓ and H and hence L are unique functions of m which allows us to calculate ℓ, m, H, L and θ as functions of x. The required functions $\ell(m)$, $H(m)$ and $L(m)$ were deduced by Thwaites from a number of exact solutions of the laminar boundary layer equations which were available to him at that time. The momentum integral equation can be integrated easily between two points x_1 and x_2 if a linear relation

$$L = a + bm \tag{32}$$

is assumed between L and m (Thwaites took $a = 0.45$; $b = 6$). The result is:

$$\left(\frac{U^b\theta^2}{\nu}\right)_{x=x_2} - \left(\frac{U^b\theta^2}{\nu}\right)_{x=x_1} = a\int_{x_1}^{x_2} U^{b-1}\, dx \tag{33}$$

As soon as $\theta(x)$ is known, $m(x)$, $\ell(x)$ and $H(x)$ follow from the compatibility condition and the relations $\ell(m)$ and $H(m)$. This allows us to find the separation point and an approximation to the boundary layer velocity profile. As was remarked already the predicted values of θ are sufficiently accurate for engineering use. For the favourable pressure gradient case ($m < 0$) also the velocity profile is rather accurate. For adverse pressure gradients ($m > 0$) the profile is less accurate and hence the separation position is not predicted accurately enough for the present purpose. This is due to the fact that Thwaites' method belongs to the class where a fixed relation exists between ℓ and m so that separation ($\ell = 0$) is found at a fixed value of m.

An improved method has been presented by Van Ingen (14) in which $\ell(m)$, $H(m)$ and hence $L(m)$ are allowed to depend on an extra parameter. This parameter is taken as m_{sep}, the value of $m = -\frac{\theta^2}{\nu}\frac{dU}{dx}$ at separation.

For each value of m_{sep} a Thwaites-type method is obtained. For large values of m_{sep} the method gives late separation, for small values of m_{sep} early separation is obtained.

Of course some additional information is needed to determine m_{sep}. When analysing experimental results this parameter may be chosen such that the experimentally determined separation point is reproduced. In cases where the separation point is not known à priori we use Stratford's two-layer method[15] in the version of Curle and Skan[16] to provide the separation position.

It is easy to invert the present method so that we can calculate the change in pressure distribution which is needed for a certain modification of the properties of the boundary layer. In this way it was shown by an example in [14] that a very minor change in pressure gradient may produce an appreciable shift in the separation position. Therefore it seems that for the prediction of the laminar separation position the accuracy of the pressure distribution is much more important than the sophistication of the calculation method. Therefore it is thought that the present method is sufficiently accurate for engineering use.

Accurate laminar boundary layer calculations for arbitrarily prescribed pressure distributions in general show a singular behaviour at separation, such that τ_0 and ℓ tend to zero as the square root of the distance to separation (Goldstein[17]). It was shown in [14] that this singular behaviour is reproduced by the present method. It was also shown that for a measured pressure distribution the singularity may be prevented by a proper choice of m_{sep}. Therefore it seems possible that the boundary layer equations may remain applicable through separation if only the proper pressure distribution is used. It should be remembered however that very small deviations from this pressure distribution will restore the singular behaviour. Therefore we must refrain from prescribing the pressure distribution in the separation region; instead we should prescribe a regular behaviour of some other quantity like τ_0, ℓ or the displacement thickness. It is of course very easy to invert the present method and prescribe a quantity other than the pressure and calculate the other boundary layer parameters and the pressure distribution in the separation region.

In order to be able to proceed in this direction we should first gather more information about the exact behaviour of the viscous flow near separation. Therefore it is useful to recall here an analytical solution of the Navier-Stokes equations which is valid in a small neighbourhood of the separation point where the inertial forces can be neglected. (See Legendre[18], Oswatitsch[19], Batchelor[20]). It follows that the separation streamline leaves the wall at an angle γ (fig. 12) which is determined by:

$$\tan(\gamma) = -3\left[\frac{\frac{d\tau_0}{dx}}{\frac{\partial p}{\partial x}}\right]_{sep} \tag{34}$$

The streamlines can easily be calculated once γ is known; they follow from:

$$y^2\left(x\tan(\gamma) - y\right) = \text{constant} \tag{35}$$

where x is the distance downstream of separation. For points at which the u-component of the velocity is zero we find $\frac{y}{x} = \frac{2}{3}\tan(\gamma)$.

405

The pressure gradient vector is at an angle $\frac{1}{3}\gamma$ with the wall and hence for shallow separation regions where γ is small the pressure gradient normal to the wall is small so that the boundary layer equations might still give a reasonable result.
Since the Goldstein singularity leads to $\frac{d\tau_o}{dx} = -\infty$ at separation, equation (34) would predict a separation angle γ of 90 degrees. This is in contradiction to experimental evidence which shows small angles γ. Therefore empirical information is needed to support the theory.
In [21] and [14] it was shown from an extensive empirical investigation that for a wide variety of separated flows it was possible to represent γ by the following simple empirical relation:

$$\tan(\gamma) = \frac{B}{\left(\frac{U\theta}{\nu}\right)_{sep}} \qquad (36)$$

where B assumed values between 15 and 20.

In [21] and [14] a simple method to calculate the separated laminar flow was introduced. In this method the shape of the separation streamline is prescribed; it leaves the wall at an angle γ determined by (36) in which B is assumed to take the value 17.5. The resulting flow is required to satisfy the von Kármán momentum integral relation, the first compatibility condition at the wall and certain relations between ℓ, m and H which follow from Stewartson's second branch solutions of the Falkner-Skan equation. The pressure distribution now follows from the computation.
It is useful to define a shape parameter g in the separated region with

$$g = \frac{y}{\theta} \qquad (37)$$

where y is the distance between the wall and the separation streamline. The x-coordinate may be non-dimensionalised as

$$x^* = \frac{x - x}{\theta_{sep} R_{\theta sep}} \qquad (38)$$

The shape of the separation streamline can be prescribed in a number of different ways. In many applications we used a straight separation streamline, leaving the wall at an angle γ given by eq. (36). The shape factor g then follows from:

$$g = \frac{B x^*}{\theta^*} \qquad (39)$$

where $\theta^* = \theta/\theta_{sep}$.
Since in most cases the separation streamline is slightly curved upwards in the laminar region a better approximation may be obtained by assuming a linear variation of g with x^* downstream of separation. Since θ is still increasing somewhat it follows that this leads, together with the linear variation of g, to a separation streamline which is slightly curved upwards. Then g follows from

$$g = B x^* \qquad (40)$$

It was conjectured from some unpublished measurements at LSL that the velocity U at the edge of the boundary layer may be - at least for engineering use - described by a universal relation between $U^* = \frac{U}{U_{sep}}$ and x^*.

It should be observed that, when it is assumed that also the shape of the velocity profile at separation is universal, the detailed development of the boundary layer downstream of separation would be universal. This would mean that g is a universal function of x^* so that B indeed should be a constant as was found from the experiments. The present version of the calculation method for separated flow at LSL uses a linear variation of g according to (40) with B = 17.5. The calculation has to stop when transition occurs either upstream or downstream of separation. In the latter case a so-called laminar separation bubble occurs which deserves some special attention. The subject of transition prediction will be discussed in section 3.4.

3.2. Bursting of the laminar separation bubble

Once the separated flow has become turbulent it may reattach as a turbulent boundary layer. However sometimes reattachment does not occur resulting in so called "bursting" of the bubble and in general a drastic change in flow behaviour. A number of methods have been developed for prediction of bubble bursting.
Owen and Klanfer[22] assumed that bursting occurs when R_{δ^*} at separation is less than 400-500. Crabtree[23] observed that there seems to be a maximum limit to the pressure rise which a reattaching turbulent shear layer may overcome. From a number of experiments he deduced that the pressure coefficient

$$\sigma = 1 - \left(\frac{U_r}{U_{sep}}\right)^2 \qquad (41)$$

is nearly constant for short bubbles about to burst; the constant value he suggested was 0.35.
If equation (41) is to be used to predict whether reattachment will occur, the value of U_r at the possible reattachment point has to be known. In a first approximation this may be taken from the pressure which would occur, without the bubble being present, at the position x_t (see fig. 13). Horton[24] gave a method to predict whether and where reattachment may occur. This method is based on the simple criterion that $\left(\frac{\theta}{U} \frac{dU}{dx}\right)_r$ = constant = -.0082 for all reattaching turbulent layers.
A simple criterion for bursting was shown by Van Ingen[14] to be provided by Stratford's zero skin friction limiting pressure distribution[25]. This is the adverse pressure distribution which a turbulent boundary layer can just negotiate without separation. This limiting pressure distribution curve, starting at the transition point T (fig. 13) can at low Reynolds number fail to cross the "inviscid pressure distribution curve". This means that the requested pressure rise is more than the Stratford pressure recovery can provide and hence bursting occurs.

3.3. Turbulent boundary layer and wake

In the present version of the LSL airfoil analysis and design program the turbulent boundary layer is calculated by means of Head's entrainment method [26]. The initial value for the momentum loss thickness θ is in general taken equal to the value for the laminar boundary layer at transition. When transition is due to roughness the value of θ may have to be increased to account for the drag of the roughness. A general procedure to take this into account has not yet been included in the program. Head's method also requires an initial value for the shape factor H. This value can either be specified by the user or it can be calculated by the program. In the latter case H is taken as the flat plate value given by Green[27] when transition occurs at or upstream of the pressure minimum. A value of H = 2 is used when a laminar separation bubble occurs. For intermediate transition positions H is interpolated linearly in m/m_{sep} between the flat plate value and 2. It appears that making H = 2 downstream of a separation bubble results in too low a drag coefficient. This is due to the fact that the present turbulent boundary layer calculation method does not account for the increased turbulence level at reattachment. It is clear that the problem of the starting conditions for the turbulent boundary layer calculation should be investigated in much more detail.

In the present program the wake is not calculated in detail. In fact it is done implicitly by means of the Squire-Young method which is used to calculate drag. The contributions of the upper and lower surface are determined separately.

Some improvement may result from replacing Head's method by the lag-entrainment method due to Green [27] which can also be used in the wake. However, it is expected that the most important improvement would result from a better description of the initial phase of the turbulent boundary layer. At LSL some research on turbulent wakes is being done by Passchier[28,29]. However this has not yet advanced to a state where improved calculation methods could be developed.

3.4. Transition prediction

In the present airfoil analysis and design program transition is predicted by means of the so called e^n method which was developed independently by Smith and co-workers[4,30] and van Ingen[5,6,32,33]. In this method linear stability theory is used to calculate the amplification of unstable disturbances in the laminar boundary layer. The streamfunction of such a disturbance is described by

$$\psi(x,y,t) = \varphi(y)\, e^{i(\alpha x - \omega t)} \qquad (42)$$

In the so-called spatial mode ω is the real frequency of the disturbance and α is a complex wavenumber

$$\alpha = \alpha_r + i\alpha_i \qquad (43)$$

This leads to a factor $e^{-\alpha_i x}$ in the disturbance

amplitude. The ratio of the amplitude a at a certain position to the amplitude a_0 when the disturbance considered is just neutrally stable follows from

$$\frac{a}{a_o} = e^\sigma \qquad (44)$$

The so-called amplification factor σ is a function of x and ω for a given boundary-layer. It can be calculated as a function of x for a series of frequencies as soon as stability diagrams are available for the velocity profiles at successive streamwise positions x. The envelope of the σ-x curves gives the maximum amplification factor σ_a for the critical frequency which is a function of x.
It was found that at the experimentally determined transition position σ_a attained nearly the same value of about 9 in many different cases. Therefore the method has become known as the e^9 method. Of course the critical value of σ_a should be a function of the free-stream turbulence and other disturbances such as sound. Therefore the method is now being referred to as the e^n method. A real problem of course is to specify n for a given windtunnel facility or for free flight. Different versions of the method have been used where the critical value of σ_a was not only varied because of the free-stream disturbances but also because improved numerical results of linear stability theory became available.
A detailed account of the development of this method at LSL has been given by van Ingen[33]. A short-cut method to predict transition in separation bubbles is also described in [33].

The present version of the method being used at Delft is based on a compilation of stability data published by Wazzan, Okamura and Smith[31], Kümmerer[34] and solutions of the Rayleigh equation for the inviscid stability of reversed flows as occurring in separation bubbles (van Ingen[14]). All these data have been reduced to a table containing about 300 members. Using this table a stability diagram can be composed for any velocity profile as soon as the critical Reynolds number is known. In the present program the critical Reynolds-number is made a known function of the parameter m/m_{sep} used in the boundary layer calculation method.
Although it is clear that the initial disturbances cannot easily be described it was tried in [33] to define a relation between the critical value σ_a and the r.m.s. value of the free-stream turbulence level Tu (in %).
From available results on transition positions on flat plates at different turbulence levels it was deduced that a good correlation for Tu > 0.1% is given by (see fig. 14)

$$\sigma_{a_1} = 2.13 - 6.18\ ^{10}\log Tu \qquad (45)$$

and

$$\sigma_{a_2} = 5.0 - 6.18\ ^{10}\log Tu \qquad (46)$$

where σ_{a_1} and σ_{a_2} correspond to the beginning and end of the transition region respectively.
For lower values of Tu such a good correlation could not be obtained. There is much more scatter

because at these low values of Tu sound distur-
bances may become the factor controlling transition
rather than turbulence. We use (45) and (46) also
for Tu < 0.1% but then Tu is considered to be an
"effective turbulence level" taking into account
also other disturbances. This leaves us with the
problem to determine Tu for a given windtunnel
facility or for free flight. At the time of
writing this paper an investigation was started
to obtain the effective Tu for different facili-
ties by comparing published transition measure-
ments with results of calculations with the
present method.
In the LSL airfoil analysis program we have to
start the turbulent boundary layer calculation
in a point rather than in a region. For the time
being we use simply as a starting point the
midpoint of the transition region. For this point
the amplification factor σ_{turb} is given by the
mean value of σ_{a1} and σ_{a2} according to equations
(45) and (46).

$$\sigma_{turb} = 3.565 - 6.18 \,^{10}\log Tu \qquad (47)$$

A further investigation is required to optimize the
choice for σ_{turb}.
As an illustration fig. 15 gives the calculated
value of the drag coefficient for the NACA 0012
airfoil as a function of σ_{turb}. It follows that
the result for $\sigma_{turb} = 9.75$ correlates well with
the measured value in the NACA low-turbulence
tunnel as given in fig. 68 of Abbott and von
Doenhoff[35]. According to equation (47) the
corresponding value for the effective turbulence
level is 0.10%. It should be noted that here we
match the calculated value for c_d with the
experimental value. This does not prove that the
transition position is predicted correctly; errors
in this prediction may be cancelled by errors in
the drag prediction. A further detailed investiga-
tion will be performed to sort this out.
For the low-turbulence tunnel at LSL we use a
somewhat lower value for Tu, namely 0.06% and
accordingly a higher value 11.2 for σ_{turb} (see
section 5).
At present an experimental program is being per-
formed in cooperation between Delft University of
Technology LSL and the Lockheed Georgia Company
in which the same airfoil model (with section
Eppler 603) will be tested in the LSL low-
turbulence tunnel and as a glove around the wing
of the Caproni motor-glider owned by Lockheed
Georgia. This program should result in a value of
σ_{turb} to be used for calculations on gliders.
Based on work by Runyan and George-Falvy[36] it
may be expected that $\sigma_{turb} = 15$ is a reasonable
approximation for glider airfoils.
For the present it is advised to use the following
values for Tu and σ_{turb}.

Facility	TU (%)	σ_{turb}
NACA LTT and similar tunnels	0.10	9.75
Advanced low turbulence tunnels such as at LSL	0.06	11.2
Free flight of gliders	0.014	15.0

3.5. An empirical correction of lift for the effects of viscosity

Due to the presence of the boundary layer the
effective shape of the airfoil changes. Moreover
the circulation is determined by the viscous flow
in the neighbourhood of the trailing-edge through
a "modified Kutta condition". The effective airfoil
shape is obtained by adding the displacement
thickness to the contour and similarly adding a
displacement tail to simulate the wake. The cor-
rected pressure distribution is then obtained from
a potential flow calculation for the modified
contour. This leads to an iterative proces. A
different method is to apply a non-zero normal
velocity on the contour and on both sides of the
dividing streamline in the wake. This second
method is favoured for panel methods because it
leaves the geometry unchanged and hence the
coefficient matrix in the resulting linear algebraic
equations is unchanged.
In the present conformal transformation method we
included a similar procedure where the normal
velocity boundary condition was applied in the
plane of the circle.
Another important effect arises from the curvature
of the streamlines in the wake (fig. 16). The
radial pressure gradient in the wake follows from

$$\frac{\partial p}{\partial r} = \frac{\rho u^2}{r} \qquad (48)$$

Since in the wake u is reduced with respect to the
potential flow value the pressure difference
across the wake will be reduced. This will lead to
a reduction in lift w.r.t. potential flow. Assuming
that the flow leaves the airfoil in the direction
of the bisector of the trailing-edge the total
turning angle will be $\alpha_c + \gamma$ (fig. 16) where α_c is
the angle of attack and γ the direction of the
trailing-edge bisector, both measured with respect
to the chord. Since the momentum loss in the wake
is represented by the drag coefficient c_d it may be
expected that the loss in lift due to wake
curvature effects may be expressed in terms of c_d
and $(\alpha_c + \gamma)$.
In the present version of the program a simple
procedure is used to correct the potential flow
value of lift for viscous effects. Since this
correction procedure is based on a limited number
of experimental results it should be used with
caution.
Originally it was tried to express the loss in lift
via a positive value of θ_{st} (see section 2.1.),
which should be determined by $(\alpha_c + \gamma)$, c_d and
$\Delta c_d = c_{du} - c_{dl}$. It was thought that the latter
parameter should be taken into account because a
difference in boundary layer thickness for upper-
and lower surface (leading to a difference for the
drag coefficient due to the upper surface (c_{du}) and
the lower surface (c_{dl}), would be simulated by a
dividing streamline leaving the upper surface.
From the available experimental results it was
impossible to find a correlation including Δc_d. In
the future we plan to investigate this point
experimentally in some detail. A symmetrical airfoil
will be induced to generate some lift at $\alpha_c = 0$ by
means of an asymmetrical roughness distribution.
In what follows we will develop the correction
procedure as it is being used at present.
It should be remembered that the lift curve slope
in potential flow is equal to

$$\left(\frac{\partial c_\ell}{\partial \alpha}\right)_{pot.flow} = 8\pi \frac{R}{c} \qquad (49)$$

and that the viscous flow value is $(1 - \varepsilon)$ times as large (see equations 23 through 27).
Figure 17 gives some results for symmetrical 4-digit airfoils at a Reynolds number of 6×10^6 in both the smooth and rough condition; the experimental results have been taken from fig. 57 of Abbott and von Doenhoff[35]; the theoretical results have been calculated using the present program. It was found that a very good approximation is given by (see fig. 18)

$$\varepsilon = 5.0 \, \tan(\delta) \, \sqrt{c_{d_o}} \qquad (50)$$

where δ is the trailing-edge angle and c_{d_o} the drag coefficient at $\alpha = 0$. Converting (50) to an expression for θ_{st} we obtain:

$$\theta_{st} = 5.0 \, \tan(\delta) \, \alpha \, \sqrt{c_d} \qquad (51)$$

For cambered airfoils we will expect a generalisation of (51) in the form:

$$\theta_{st} = 5.0 \, \tan(\delta) \, (\alpha_c + \gamma) \, \sqrt{c_d} \qquad (52)$$

In fig. 19 we present some results for different cambered airfoils tested in the LSL low turbulence tunnel.

Included are the points of fig. 18 but now converted to θ_{st} values for $\alpha_c = 2.0$ using equation 51. Although the correlation is good the authors are still a bit puzzled about the influence of Δc_d they expected. As mentioned already this point will be the subject of further research at LSL.

4. Experimental facilities for airfoil research at LSL

Measurements on airfoils have been performed at LSL in the low speed low turbulence tunnel. The test section of this tunnel is 1.80 m wide and 1.25 m high; the contraction ratio is 1 : 16. The maximum speed is about 120 m/sec; the r.m.s. value of the streamwise turbulent velocity fluctuation ranges from 0.025% at low speeds to 0.085% at 100 m/sec. The value of the effective turbulence level Tu mentioned in section 3.4. is about 0.06%. Typical 2-D airfoil models used in this tunnel have a chord of 0.36 m (giving a tunnel width-chord ratio of 5) and span the 1.25 m height of the tunnel. Due to a specially developed technique of casting models (van Heuven[37]) it is relatively easy to build models with a sufficient number of pressure orifices to obtain detailed pressure distributions. The drag is determined from measurements in the wake following the procedure described by Pfenninger[38]. The lift is determined from the pressure distribution on the airfoil or in special cases from the pressure distribution on the side walls of the tunnel. With these models chord Reynolds numbers between 0.5×10^6 and 2.0×10^6 are obtained.
For measurements at lower Reynolds numbers between

40 000 and 500 000 smaller models are used with a chord of 0.15 m and a span of 0.75 m. One tip of such a model is attached to the windtunnel balance system with a reflection plate normally used for half-model testing. At the other tip an end plate is provided separated from the airfoil by a narrow slot of about 0.5 mm.
The drag is again determined with the wake traverse method; the lift is measured with the balance system.

The techniques used to determine transition, separation and reattachment include stethoscope measurements, surface flow visualisation using the oil film technique and flow field explorations with tufts.
A description of this test technique has been given by Volkers[39].
The same set-up has been used by Bruining[45] to determine the aerodynamic characteristics of curved plates.

5. Some comparisons between theory and experiment

Fig. 20 shows the theoretical and experimental lift and drag for the Wortmann FX66-S-196V1 airfoil. The experimental results have been obtained by Gooden [41,42] in the low turbulence tunnel at LSL.
It was found that a good prediction of the lower limit of the low drag bucket was obtained for Tu = 0.06 (σ_{turb} = 11.2). These same values will be used for all subsequent calculations to compare with experimental results from the LSL tunnel.
A reasonable prediction of c_d and a good prediction of c_ℓ below $c_{\ell_{max}}$ is obtained.
Fig. 21 shows similar results for the FX61-163 airfoil as used in the ASW-19 sailplane. The experimental results have been obtained by Selen et. al [43] in the LSL tunnel.
Fig. 22 shows results for an airfoil which is used in the horizontal tailplane of the Italian sailplane M300 "Aliante". The airfoil was designed by cambering the NACA 63-018 section. The tailplane was produced through an extrusion proces which caused appreciable surface waviness. An actual specimen of this tailplane was tested as a two-dimensional model in the LSL tunnel. It was found that the surface waviness caused early transition in a certain angle of attack range. This could be remedied by smoothing the forward part of the surface. The calculation, starting from measured airfoil coordinates for both conditions, predicted this change quite well.
Fig. 23 shows the calculated drag coefficient for symmetrical NACA 4-digit airfoils as a function of thickness at a chord Reynoldsnumber of 6×10^6 for both the smooth and rough condition. The experimental results indicated in the figure have been taken from fig. 68 of [35]. For the calculations the same values for Tu (= 0.1) and σ_{turb} (= 9.75) have been used as were obtained in section 3.4. (fig. 15) for NACA 0012 in the smooth condition. To simulate the effect of the standard roughness a non-dimensional value of the momentum loss thickness ($\theta^* = \frac{\theta}{c} \sqrt{R_c}$) at 8% chord was chosen for NACA 0012 to match the experimental value of c_d. For the other thicknesses θ^* was kept equal.
Fig. 24 shows lift and drag for the NACA 64_2-415 airfoil at $R_c = 3 \times 10^6$ and 9×10^6. The experimental results follow from [35]; the calculations have been performed for Tu = 0.1 and σ_{turb} = 9.75.
Fig. 25 shows the experimental lift curves for the FX66-S-196V1 airfoil at very low Reynolds numbers obtained by Volkers[39] in the LSL tunnel.

It should be noted that at a moderate angle of attack, say $\alpha_c = 5^o$, bursting of the laminar separation bubble is indicated by a sudden loss of lift below $R_c = 0.25 \times 10^6$. It should be mentioned that this critical Reynolds number is far below the design value for this airfoil. Finally fig. 26 shows the result of the bursting prediction for this case using Stratfords limiting pressure distributions. It follows that bursting is predicted for a Reynoldsnumber of about 0.16×10^6.

6. Concluding remarks

It has been shown that a reasonable prediction of the lift and drag characteristics of airfoils for low speed applications can be made. The programs which are now available at LSL will be used in the near future to design improved airfoils for sailplanes. The specifications for the airfoils to be designed will follow from the parametric sailplane performance optimization programs which have been developed by Boermans[46,47].

7. References

1. Timman, R.: The direct and inverse problem of aerofoil theory. A method to obtain numerical solutions. National Aerospace Laboratory NLR, Amsterdam, report NLL-F16 (1951).
2. Ingen, J.L. van: Advanced computer technology in aerodynamics: a program for airfoil section design utilizing computer graphics. Lecture notes for Von Karman Institute of Fluid Dynamics (1969), AGARD lecture series no. 37 "High Reynolds-number subsonic aerodynamics", p. 8.1-8.33 (1970).
3. Ingen, J.L. van: On the design of airfoil sections utilizing computer graphics. De Ingenieur, jrg. 81 no. 43, p. L110-L118 (1969).
4. Smith, A.M.O., Gamberoni, N.: Transition, pressure gradient, and stability theory. Douglas Aircraft Co., report ES 26388 (1956).
also: Smith, A.M.O.: Transition, pressure gradient, and stability theory. Proc. 9th Int. Congr. Appl. Mech., Brussels, 4, p. 234-244 (1956).
5. Ingen, J.L. van: Een semi-empirische methode voor de bepaling van de ligging van het omslaggebied van de grenslaag bij onsamendrukbare tweedimensionale stromingen. Delft University of Technology, dept. of Aerospace Engineering, report VTH-71 (1956).
6. Ingen, J.L. van: A suggested semi-empirical method for the calculation of the boundary layer transition region. Delft University of Technology, Dept. of Aerospace Engineering, report VTH-74 (1956).
7. Müller, W.: Zur Konstruktion von Tragflächenprofilen. Z.A.M.M. 4, p. 213-231 (1924).
8. Blom, J.J.H.: Beschrijving van een vijfparameter profielfamilie. Delft University of Technology, dept. of Aerospace Engineering, report LR-220 (1976).
9. Theodorsen, T.: Theory of wing sections of arbitrary shape. NACA Report 411 (1932).
10. Goldstein, S.: Approximate two-dimensional aerofoil theory. Parts I-VI, A.R.C.-CP 68-73 (1952).
11. Lighthill, M.J.: A new method of two-dimensional aerodynamic design. R and M 2112 (1945).
12. Gooden, J.H.M.: A numerical method of calculating two-dimensional windtunnel wall interference on multi-element airfoils in incompressible, inviscid flow. Delft University of Technology, Dept. of Aerospace Engineering, report to be published.
13. Thwaites, B.: Approximate calculation of the laminar boundary layer. Aeron. Quart., 1, p. 245-280 (1949).
14. Ingen, J.L. van: On the calculation of laminar separation bubbles in two-dimensional incompressible flow. In AGARD CP-168: "Flow Separation", Göttingen (1975).
15. Stratford, B.S.: Flow in the laminar boundary layer near separation. R and M 3002 (1957).
16. Curle, N. and Skan, S.W.: Approximate methods for prediction separation properties of laminar boundary layers. Aeron. Quart., 8, p. 257-268. See also: Curle, N.: The estimation of laminar skin friction, including the effects of distributed suction. Aeron. Quart., 11, p. 1-21 (1960).
17. Goldstein, S.: On laminar boundary layer flow near a position of separation. Quart. J. Mech. Appl. Math. Vol 1, p. 43-69 (1948).
18. Legendre, R.: Décollement laminaire régulier. Comptes Rendus 241, p. 732-734 (1955).
19. Oswatitsch, K.: Die Ablösungsbedingung von Grenzschichten. In: Grenzschichtforschung/Boundary layer research. IUTAM Symposium, Freiburg/Br. 1957, Springer Verlag 1958, p. 357-367.
20. Batchelor, G.K.: An introduction to fluid dynamics. Cambridge Univ. Press (1970).
21. Dobbinga, E., Ingen, J.L. van, Kooi, J.W.: Some research on two-dimensional laminar separation bubbles. AGARD CP-102, paper nr. 2, Lisbon (1972).
22. Owen, P.R. and Klanfer, L.: On the laminar boundary layer separation from the leading-edge of a thin airfoil. ARC-CP 220 (1955).
23. Crabtree, L.F.: The formation of regions of separated flow on wing surfaces. R and M 3122 (1959).
24. Horton, H.P.: A semi-empirical theory for the growth of laminar separation bubbles. ARC-CP 1073 (1967).
25. Stratford, B.S.: The prediction of separation of the turbulent boundary layer. Journal of Fluid Mechanics, Vol 5, pt. 1, January 1959, p. 1-16.
26. Head, M.R.: Entrainment in the turbulent boundary layer. R and M 3152 (1958).
27. Green, J.E., Weeks, D.J. and Brooman, J.W.F.: Prediction of turbulent boundary layers and wakes in compressible flow by a lag-entrainment method. R and M 3791 (1977).
28. Passchier, D.M.: Some measurements in the wake behind a circular cylinder. Delft University of Technology, Dept. of Aerospace Engineering, report LR-229 (1977).
29. Passchier, D.M.: A calculation method for the incompressible two-dimensional turbulent wake with streamwise pressure gradient. Delft University of Technology, Dept. of Aerospace Engineering, report LR-230 (1977).
30. Jaffe, N.A., Okamura, T.T. and Smith, A.M.O.: Determination of spatial amplification factors and their application to predicting transition. AIAA Journal, Vol 8, no. 2, February 1970, p. 301-308.
31. Wazzan, A.R., Okamura, T.T. and Smith, A.M.O.: Spatial and temporal stability charts for the Falkner-Skan boundary layer profiles. DAC 67086, sept. 1968, McDonnel Douglas Corp.
32. Ingen, J.L. van: Theoretical and experimental investigations of incompressible laminar boundary layers with and without suction. Report VTH-124, Delft University of Technology, Dept. of Aerospace Engineering (1965).
33. Ingen, J.L. van: Transition, pressure gradient, suction, separation and stability theory. In AGARD CP-224: Laminar-Turbulent Transitions, Copenhagen (1977).
34. Kümmerer, H.: Numerische Untersuchungen zur

Stabilität ebener laminarer Grenzschichtströmungen. Dissertation Technische Hochschule, Stuttgart (1973).

35. Abbott, I.H. and von Doenhoff, A.E.: Theory of wing sections. Dover, New York (1959).

36. Runyan, L.J. and George-Falvy, D.: Amplification factors at transition on an unswept wing in free flight and on a swept wing in windtunnel. AIAA paper 79-0267 (1979).

37. Heuven, M.H.W. van: Een relatief goedkope methode voor de fabricage van twee-dimensionale kunststof windtunnelmodellen met ingegoten druk-leidingen. Delft University of Technology, Dept. of Aerospace Engineering, report LR-202 (1975).

38. Pfenninger, W.: Vergleich der Impulsmethode mit der Wägung bei Profilwiderstandsmessungen. Mitteilung 8 der ETH, Zürich (1943).

39. Volkers, D.F.: Preliminary results of wind-tunnel measurements on some airfoil sections at Reynolds numbers between 0.6 $\times$ 10^5 and 5.0 $\times$ 10^5. Delft University of Technology, Dept. of Aerospace Engineering, Memorandum M-276 (1977).

40. Taghavi, H. and Wazzan, A.R.: Spatial stability of some Falkner-Skan profiles with reversed flow. Physics of Fluids, Vol. 17, no. 12, Dec. 1974, p. 2181-2183.

41. Gooden, J.H.M.: Experimental low-speed aero-dynamic characteristics of the Wortmann FX66-S-196V1 airfoil. To be published as a Report by Delft University of Technology, Dept. of Aerospace Engineering.

42. Gooden, J.H.M.: Experimental low-speed aero-dynamic characteristics of the Wortmann FX66-S-196V1 airfoil (Paper presented at the XVI OSTIV Congress, Chateauroux, France, 1978). Technical Soaring, Vol. 5, no. 3.

43. Selen, H.J.W., Wijnheijmer, M.L. and Boermans, L.M.M.: Windtunnel tests of two wing segments of the ASW-19 sailplane. To be published as Memo-randum M-   , Delft University of Technology, Dept. of Aerospace Engineering (1980).

44. Boermans, L.M.M. and Blom, J.J.H.: Low-speed aerodynamic characteristics of an 18% thick air-foil section designed for the all-flying tailplane of the M-300 sailplane. Delft University of Technology, Dept. of Aerospace Engineering, report LR-226 (1976).

45. Bruining, A.: Aerodynamic characteristics of a curved plate airfoil section at Reynoldsnumbers 60.000 and 100.000 and angles of attack from -10 to +90 degrees. Delft University of Technology, Dept. of Aerospace Engineering, Report LR-281 (1979).

46. Boermans, L.M.M.: Development of a computer program for parametric sailplane performance optimization. Presented at the XVI OSTIV Congress, Chateauroux, France (1978), Aero-Revue 5,6/1980.

47. Boermans, L.M.M.: Soaring flight optimization theory and an application in sailplane design. NVvL-Annual Report (1978).

48. Schubauer, G.B. and Skramstad, H.K.: Laminar boundary layer oscillations and transition on a flat plate. NACA Report 909 (1948).

49. Hall, D.J. and Gibbings, J.C.: Influence of stream turbulence and pressure gradient upon boundary layer transition. Journal Mechanical Engineering Science, Vol. 14, no. 2, p. 134-146 (1972).

Fig. 1: Classical conformal transformations (table 1).
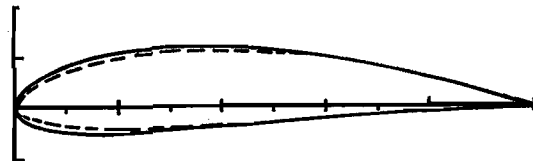
Fig. 2: Comparison of von Kármán-Trefftz (----) and Müller airfoil (——) for $\delta = 18°$; $\beta = 4.737°$ and $\dfrac{b}{R} = 0.931$.
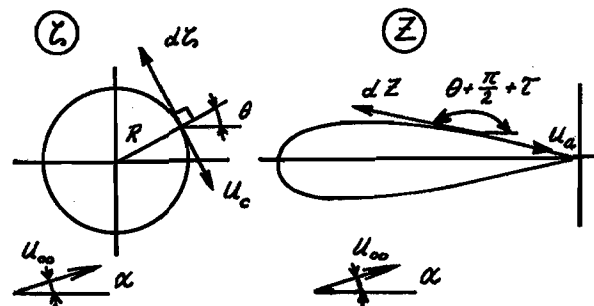
Fig. 3: Conformal transformation according to Timman.
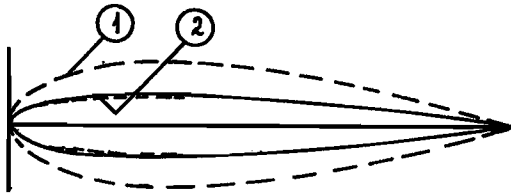
Fig. 4: Finding the transformation for NACA 0012;
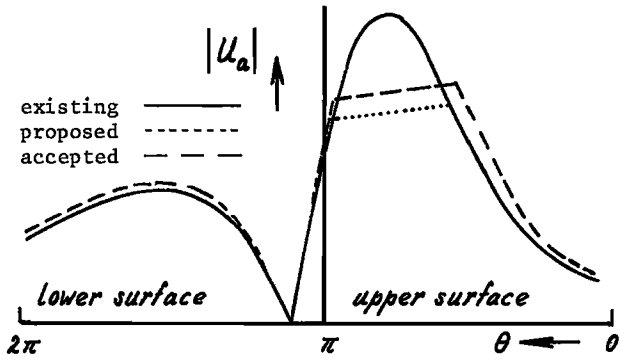①, ② = first and second approximation; ——— =
NACA 0012.

existing ———
proposed ·········
accepted — — —

$|u_a|$

lower surface   upper surface

2π π $\theta \longleftarrow 0$

Fig. 5: Obtaining airfoils with improved pressure
distributions.

$|u_a|$

.8
.6
.4
.2

2π π $\theta \longleftarrow 0$
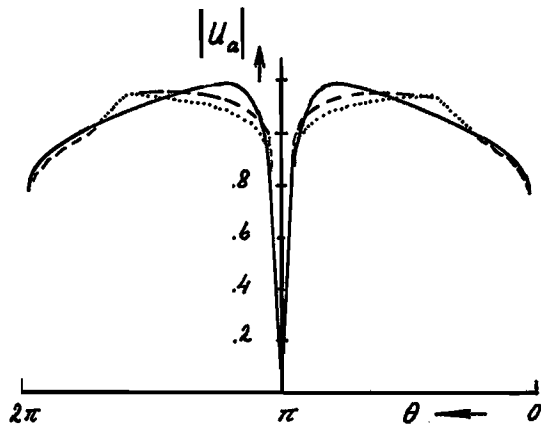
Fig. 6: Modifying NACA 0012 pressure distribution
into one of laminar flow type; existing (NACA 0012)
————; proposed ·········; accepted — — —.

Fig. 8: Transforming the Eppler 377 airfoil into a
near circle.
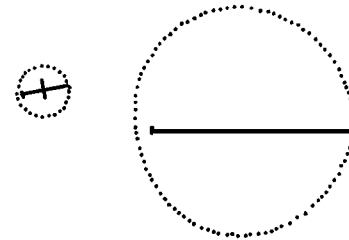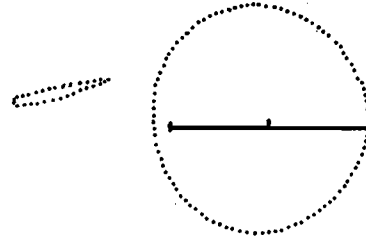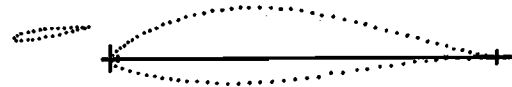
Fig. 9: Transformation of NACA 0012 leading-edge
slat and FX66-S-196V1 main airfoil into two nearly
circular contours.
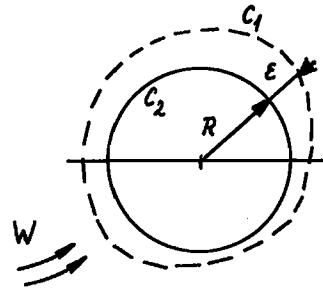
Fig. 10: Contour C_1 and circle C_2.

Fig. 7: Transforming the Wortmann FX66-S-196V1 air-
foil into a near circle.
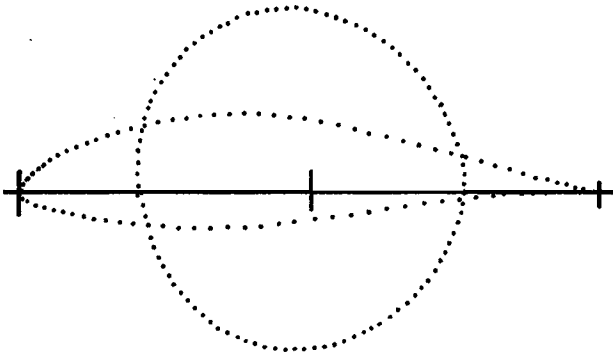
Fig. 11: Singularity distributions on circle with radius R = 1 to generate the flow around ellips with axes a and b.
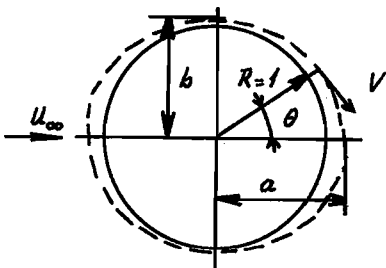
Fig. 12: Separation angle γ.

Fig. 15: c_d as function of σ_{turb} for NACA 0012; R_c = 6 x 10⁶ smooth condition.

Fig. 13: Schematics of separation bubble.
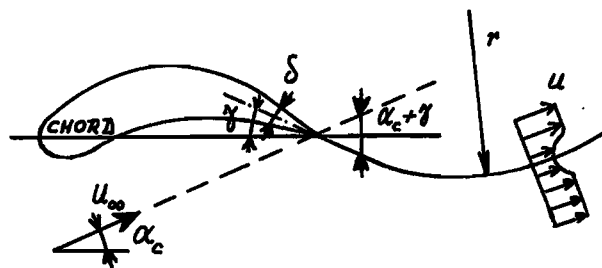
Fig. 16: Wake curvature parameters.

Fig. 14: Relation between σ_a and Tu for flat plate.
—·— ref. 48; —··— ref. 49.
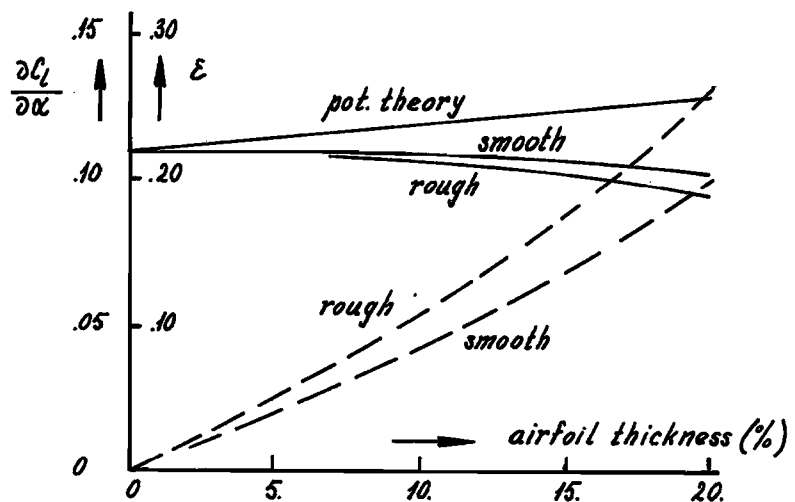
Fig. 17: $\frac{\partial c_\ell}{\partial \alpha}$ and ε for symmetrical NACA 4-digit airfoils; R_c = 6 x 10⁶; ——— $\frac{\partial c_\ell}{\partial \alpha}$; ----- ε; expt. values according to (35).

413
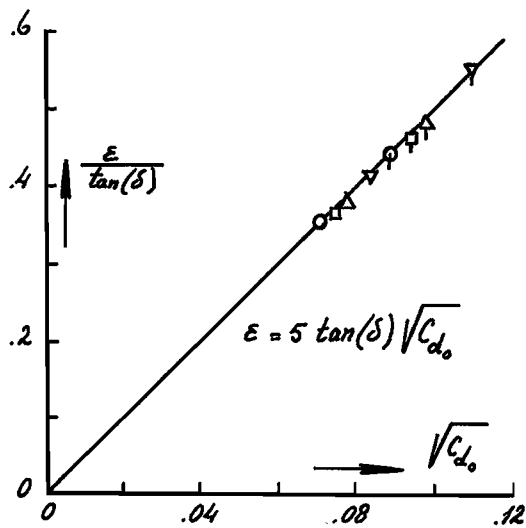
Fig. 18: ε for symmetrical NACA 4-digit airfoils;
$R_c = 6 \times 10^6$, $\odot$ = NACA 0006; $\boxdot$ = 0009; $\triangle$ = 0012;
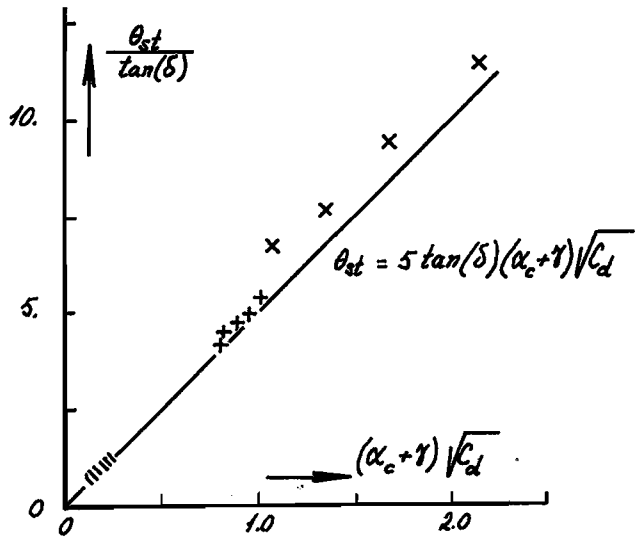∇ = 0020. Flagged symbols denote standard roughness.

Fig. 19: θ_{st} for different airfoils; $\backslash\backslash\backslash\backslash\backslash$= 4-digit
from fig. 18; $+$ = FX 66-S-196V1, α_c = 0, R_c = 0.5 x
10^6 to 2.0 x 10^6; $\times$ = FX 61-163, R_c = 1.5 x 10^6,
$-4 < \alpha_c < 7$.
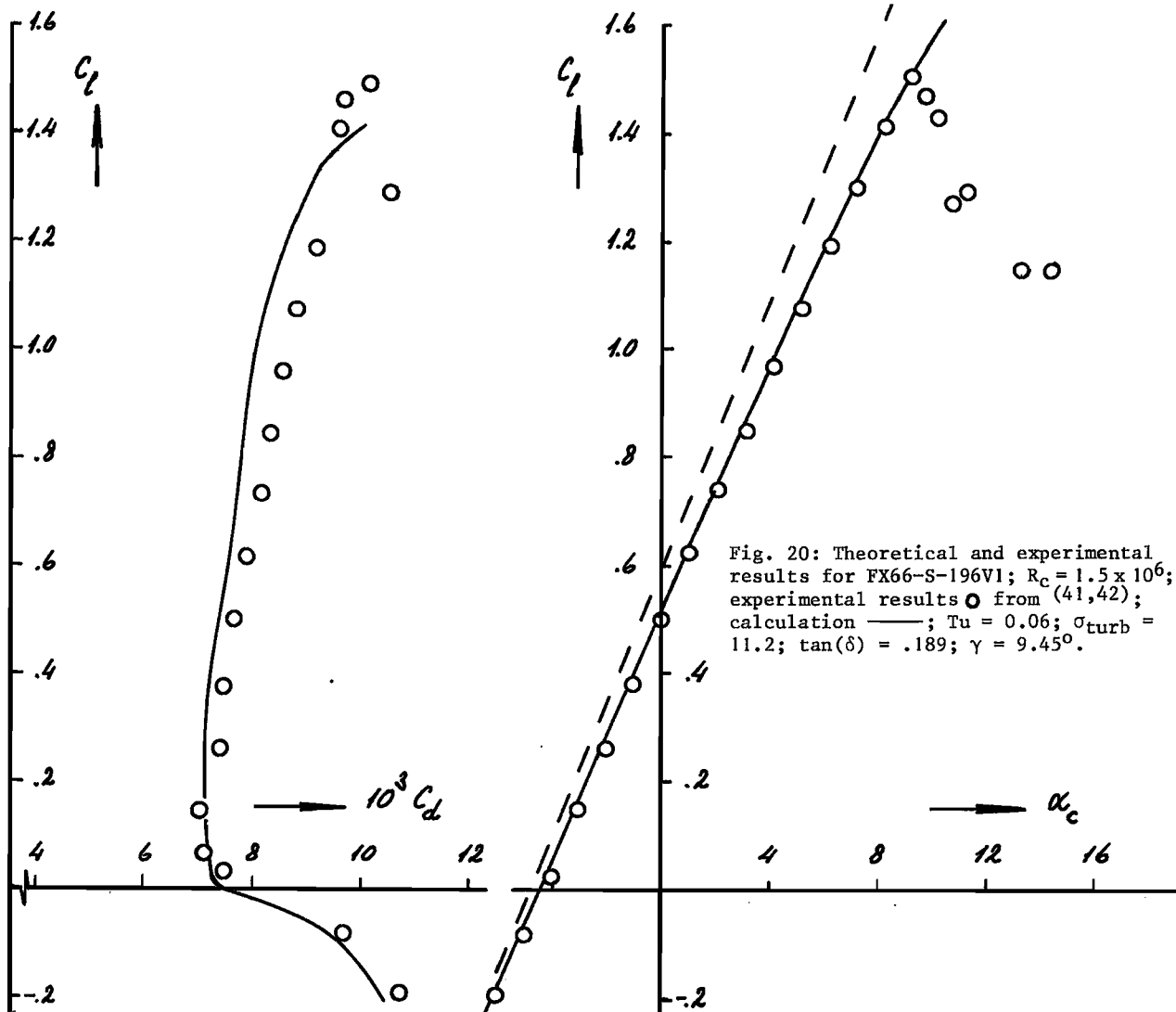
Fig. 20: Theoretical and experimental
results for FX66-S-196V1; $R_c = 1.5 \times 10^6$;
experimental results $\mathbf{O}$ from (41,42);
calculation ——; Tu = 0.06; σ_{turb} =
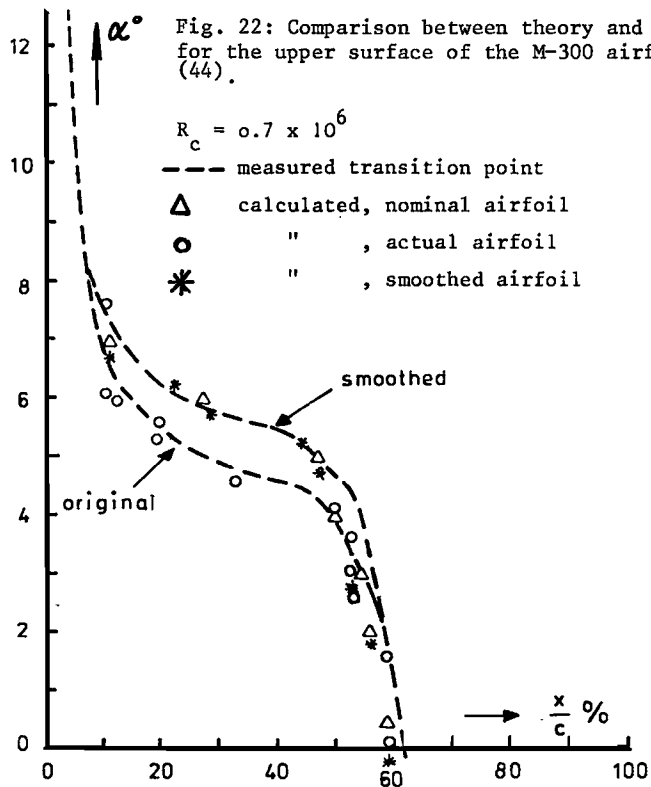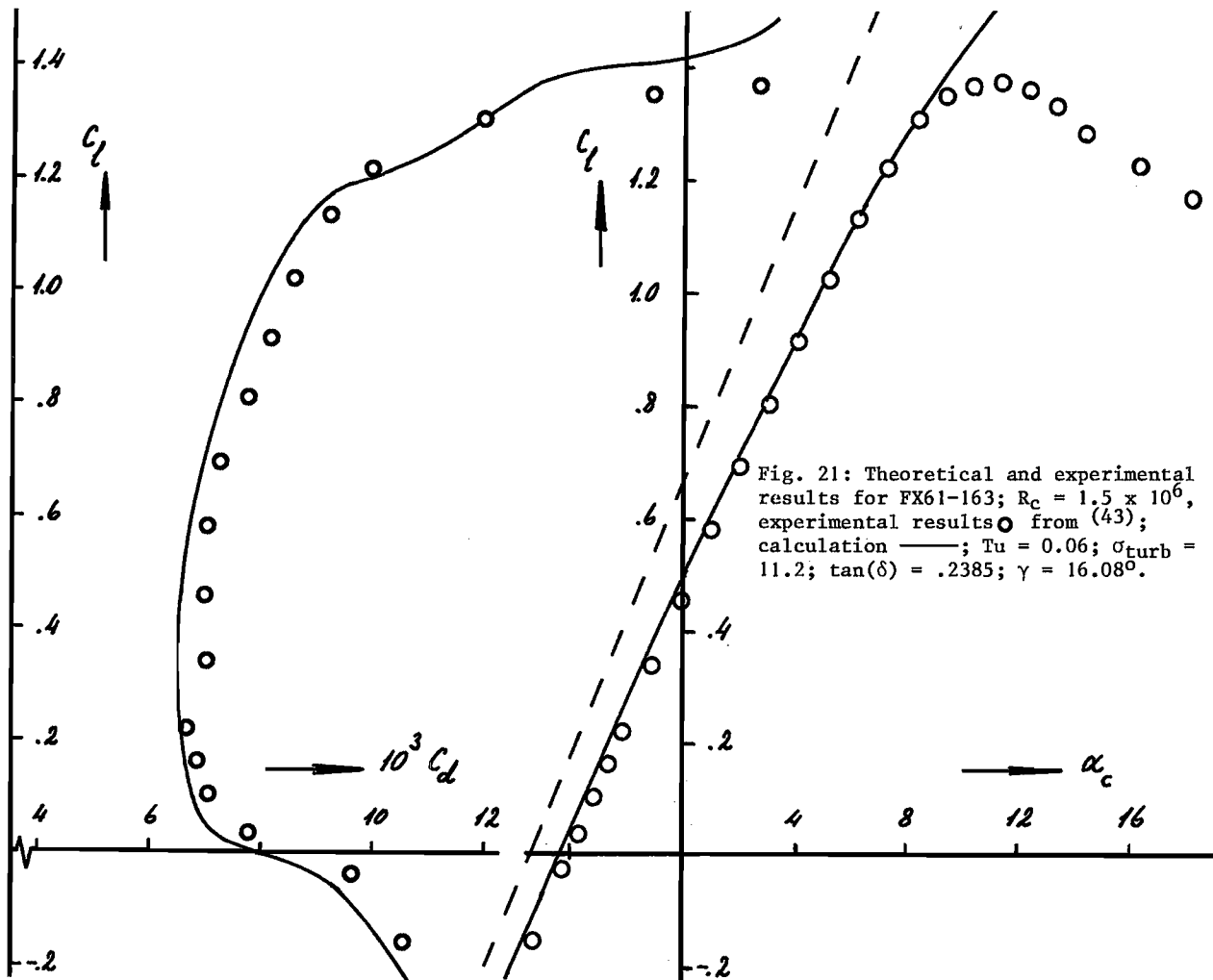11.2; $\tan(\delta)$ = .189; γ = 9.45°.

414

Fig. 21: Theoretical and experimental results for FX61-163; $R_c = 1.5 \times 10^6$, experimental results ○ from [43]; calculation ——; $Tu = 0.06$; $\sigma_{turb} = 11.2$; $\tan(\delta) = .2385$; $\gamma = 16.08°$.

Fig. 22: Comparison between theory and experiment for the upper surface of the M-300 airfoil, from [44].

$R_c = 0.7 \times 10^6$

——— measured transition point

△ calculated, nominal airfoil

○ " , actual airfoil

✳ " , smoothed airfoil

Fig. 23: c_d as function of thickness ratio for symmetrical NACA 4-digit airfoils at $R_c = 6 \times 10^6$, calculation for $Tu = 0.1\%$, $\sigma_{turb} = 9.75$; —— = smooth; ----- = rough; ○ = expt. according to [35].
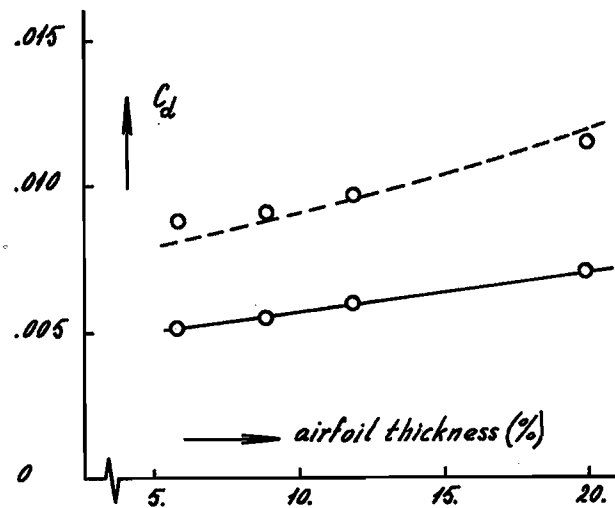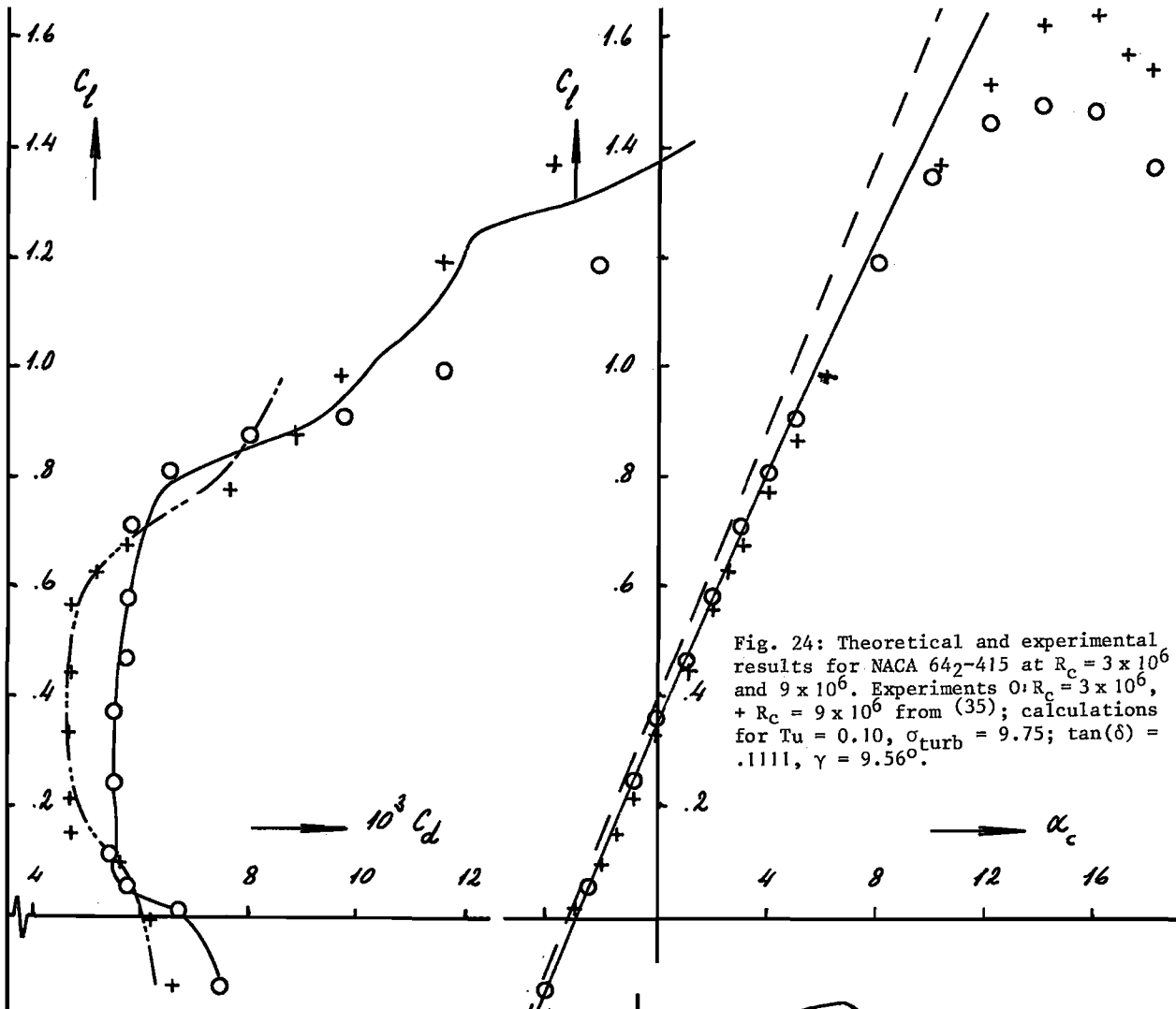
Fig. 24: Theoretical and experimental results for NACA 64_2-415 at $R_c = 3 \times 10^6$ and 9×10^6. Experiments O: $R_c = 3 \times 10^6$, + $R_c = 9 \times 10^6$ from [35]; calculations for Tu = 0.10, σ_{turb} = 9.75; tan(δ) = .1111, γ = 9.56°.
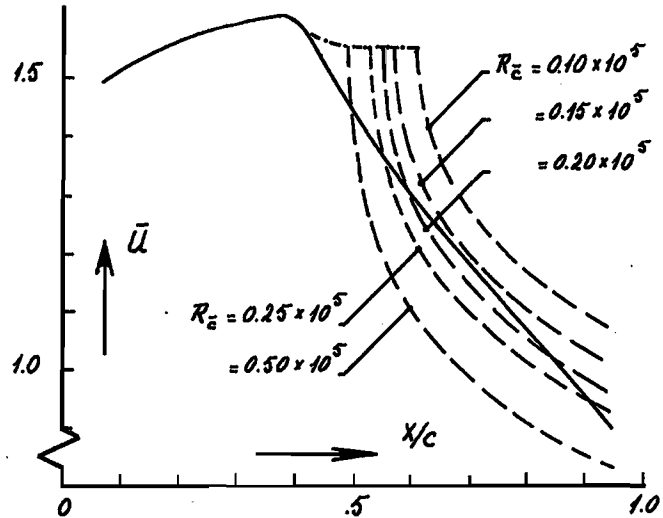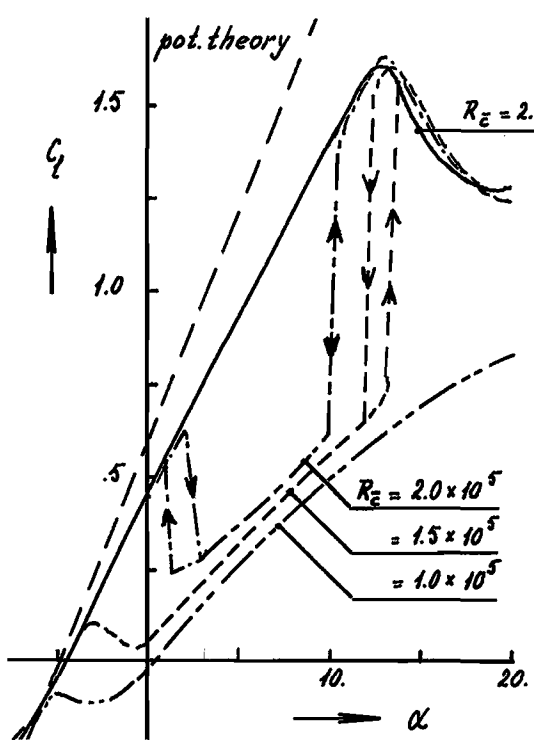
Fig. 26: Prediction of bursting at α_c = 5° for FX66-S-196V1 using Stratfords limiting pressure distributions; ——— = pressure distribution without bubble; —·— = laminar part of bubble, calculated for B = 17.5; ———— = Stratford.

Fig. 25: Experimental lift curves at very low Reynolds numbers for FX66-S-196V1 taken from Volkers (39).

416